Environ Fluid Mech (2018) 18:807–828
https://doi.org/10.1007/s10652-017-9561-9

ORIGINAL ARTICLE

# Turbulence and turbulent flux events in tidal bores: case study of the undular tidal bore of the Garonne River

**Xinqian Leng**[1] · **Hubert Chanson**[1] · **David Reungoat**[2,3]

Received: 8 June 2017 / Accepted: 10 November 2017 / Published online: 17 November 2017


**Abstract** The tidal bore of the Garonne River (France) was investigated on 29 August, 31 August and 27 October 2015, during which instantaneous velocity measurements were performed continuously at high-frequency (200 Hz). The tidal bore occurrence had a marked effect on the flow field and turbulent Reynolds stress data, indicating large shear stresses, together with large and rapid fluctuations, during the bore passage and the early flood tide. Like many natural process flows, the tidal bore flow motion was dominated by coherent structure activities and turbulent events, with significant impact on the natural systems including in terms of sediment processes. Herein a new turbulent event analysis was developed for the highly-unsteady rapidly-varied tidal bore flow. The analysis was based upon basic concepts, in which turbulent bursting events were defined in terms of the instantaneous relative turbulent flux, and the method was extended to the rapidly-varied, highly-unsteady tidal bore motion. The turbulent event data showed relatively close results for most fluxes during the tidal bores. The event duration showed some tidal trend, with longer turbulent events immediately after the tidal bore passage, occurring simultaneously with major sediment erosion processes. The field data set and analyses suggested that a turbulent event analysis may be applicable to highly-unsteady rapidly-varied flows, providing quantitative details into the turbulent bursts that are responsible for major mixing and sedimentary processes.

**Keywords** Turbulent flux events · Turbulent momentum flux · Unsteady turbulence · Compression wave · Tidal bore · Field observations · Suspended sediment processes

✉ Hubert Chanson
h.chanson@uq.edu.au

[1] School of Civil Engineering, The University of Queensland, Brisbane, QLD 4072, Australia

[2] I2M, Laboratoire TREFLE, Université de Bordeaux, 16 avenue Pey-Berland, Pessac, France

[3] CNRS UMR 5295, 33607 Pessac, France

## 1 Introduction

Many turbulent flows are often dominated by coherent structure activities and turbulent events, since turbulence is not a Gaussian process [1], in particular in Nature. A turbulent event may be defined as a series of turbulent fluctuations that contain more energy than the average turbulent fluctuations within a studied data section [15, 29, 38]. Turbulent event analyses were successfully applied to laboratory open channel flows [13, 19], water tunnel investigations [12], wind tunnel studies [25], atmospheric boundary layer flows [8, 20], estuarine flows [35], as well as direct numerical simulation (DNS) investigations of boundary layers [18]. Such turbulent event analyses were developed for steady flows and were never applied to unsteady rapidly-varied open channel flows like tidal bores (Fig. 1), except possibly a quadrant analysis conducted by Reungoat et al. [31].

A tidal bore is a compressive wave of tidal origin, propagating upstream as the tidal flow turns to rising when a macro-tidal flood flow enters a funnel shaped estuary with shallow waters [2, 36]. Figure 1 shows the tidal bores of the Qiantang and Dordogne Rivers. The strength of a tidal bore is characterised by its Froude number $Fr_1$. A breaking bore is observed for $Fr_1 > 1.4$–$1.7$ (Fig. 1a), while a undular bore is seen for $Fr_1 < 1.3$–$1.5$ (Fig. 1b). The occurrence of tidal bores has a significant impact on the natural systems, the bore propagation being associated with sediment scouring and massive suspension of bed materials [6, 11]. The passage of tidal bores was found to place into suspension large amounts of fine sediments, which were advected in the wake of the bore front [5, 39]. In-situ observations were reported in both small rivers [9, 34] and large estuarine systems [7, 14].

In the present study, field measurements were conducted in the tidal bore of the Garonne River (France) at the same site on 29 August 2015, 31 August 2015 and 27 October 2015. On each day, instantaneous velocity measurements were performed continuously at high-frequency (200 Hz) prior to, during and after each afternoon tidal bore. A detection of turbulence bursting events was developed based upon the technique of Narasimha et al. [20]. The approach was found to be well-suited to highly-unsteady rapidly-varied tidal bore flows, and provided insights into the interplay between turbulent and sedimentary processes in the large-scale environmental system.

## 2 Field investigation, instrumentation and data analyses

### 2.1 Field investigation and instrumentation

Field measurements were performed in the tidal bore of the Garonne River (France), at a site previously used by Chanson et al. [5], Reungoat et al. [30] and Keevil et al. [14]. The study Chanson et al. [5] was primarily a proof of concept, while ADV operational issue was experienced and only part of entire data sets was useable. The work by Reungoat et al. [30] was conducted shortly after a major flood, showing some most unusual delayed flow reversal during the bore passage. The work of Keevil et al. [14] put some emphasis on the suspended sediment processes, based upon some relatively low-frequency instrumentation, i.e. optical backscatter (OBS) data collected at 25 Hz, time-averaged for 5 s, and provided every 10 s. Herein both velocity and suspended sediment concentration (SSC) data were collected at relatively high-frequency (200 Hz), enabling some detailed turbulent event analysis (see below).

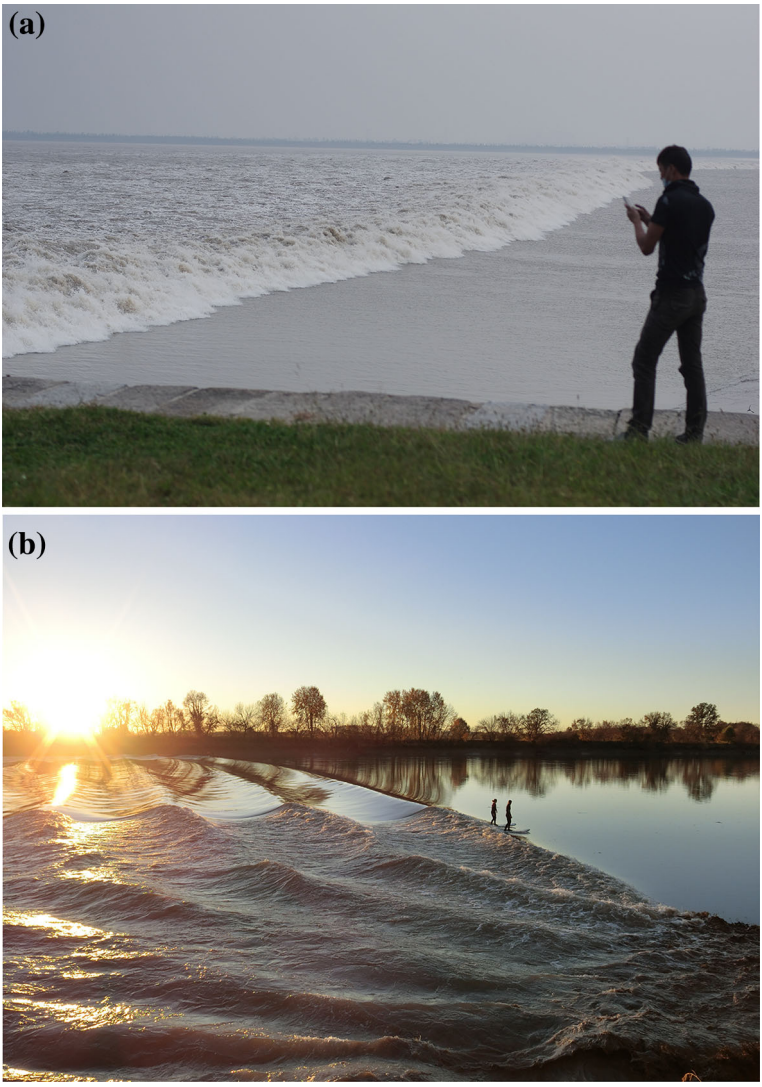


**Fig. 1** Photographs of tidal bores in rivers. **a** Breaking tidal bore of the Qiantang River on 11 October 2014 between Yanguan and Laoyanchang (China)—bore propagation from left to right—the bore front was about 3–4 m and its width in excess of 2 km, **b** undular tidal bore of the Dordogne River upstream of Libourne (France) on 1 November 2015

The sampling site is located 102.3 km upstream of the river mouth (Pointe de Grave) and 6.5 km upstream of Bordeaux city (Fig. 2a, Left). The Arcins channel is 1.8 km long, 70 m wide and about 1.1–2.5 m deep at low tide, between the Arcins Island and the river's right bank (Fig. 2b). Figure 2a shows a map of the area and Fig. 2b a photograph of the undular bore shortly before reaching the sampling location. Figure 2c presents some survey data, with z being the vertical elevation in m NGF IGN69. The NGF IGN69 uses the Nivellement General de la France suitable for France, the datum being determined by the Marseille tidal gauge. Detailed field measurements were conducted under spring tide

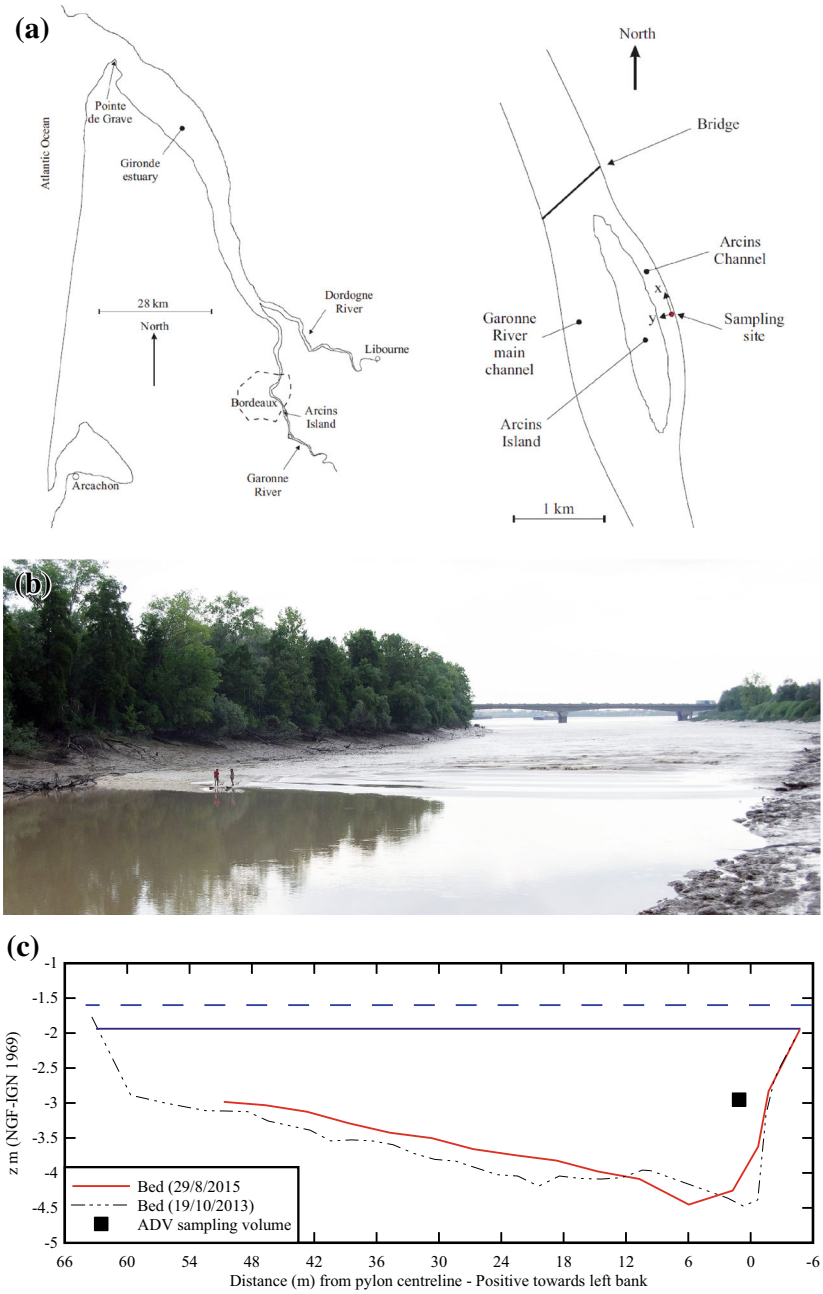


**Fig. 2** Details of the sampling site location in the Arcins Channel, Garonne River (France). **a** Map of south-western France (France) (Left) and of Arcins Channel (Right), **b** undular tidal bore in the Arcins Channel on 31 August 2015 afternoon—note some breaking next to the left bank (left of surfers), **c** surveyed channel cross-section on 29 August 2015 looking downstream—water levels immediately before (solid line) and after (dashed line) the tidal bore front are shown, with the ADV control volume before bore passage (black square, for the 29 August 2015—comparison with bed elevations surveyed on 19 October 2013

conditions on 29 August, 31 August and 27 October 2015, with a tidal range between 5.85 and 6.32 m, and tidal bore Froude numbers between 1.18 and 1.7 (Table 1). Table 1 summarises the initial flow conditions (subscript 1) as well as the bore celerity U and conjugate water depth $d_2$. All measurements were started prior to the passage of the tidal bore and ended at least 1 h after the bore passage. Although the tides are semi-diurnal, the tidal data indicated slightly different periods and amplitudes typical of diurnal inequality.

On each day, free surface elevations were recorded using a survey staff, while instantaneous velocity components were measured using a Nortek$^{TM}$ Vectrino + acoustic Doppler velocimeter (ADV) equipped with a down-looking head. The ADV unit was fixed beneath a heavy pontoon and its control volume was located 1.0 m below the free-surface. The instrument was fixed on a frame attached to the very sturdy pontoon, of more than 30 m long, used to receive boats of over 25 tons displacement. The aluminium frame was solidly fixed underwater and rubber pads were used to prevent any vibrations. The ADV system was sampled continuously at 200 Hz without interruption, starting at least 1 h before and ending at least 1 h after the bore passage. The velocity signal post-processing included the removal of communication errors, the removal of average signal to noise ratio (SNR) data less than 5 dB, the removal of average correlation values less than 60% and despiking using the phase-space thresholding technique [10, 37]. The percentage of good samples ranged between 79 and 85% for the entire data sets. The suspended sediment concentration was derived from the ADV signal amplitude after a careful calibration, and checked against water samples collected during the field studies [32]. The sediments were some cohesive mixture, basically including about 10% clay, 88% silt and 2% sand, with a median grain size between 10 and 20 μm. Further details are reported in Reungoat et al. [32].

**Table 1** Field measurements in the tidal bore of the Garonne River in the Arcins channel (France)

| Reference | Date | Tidal range (m) | U (m/s) | $V_1$ (m/s) | $d_1$ (m) | $d_2$ (m) | $A_1$ ($m^2$) | $B_1$ (m) | $Fr_1$ |
|---|---|---|---|---|---|---|---|---|---|
| (1) | (2) | (3) | (4) | (5) | (6) | (7) | (8) | (9) | (10) |
| Present study | 29/08/2015 | 5.85 | 4.23 | 0.29 | 1.685 | 2.023 | 101.4 | 67.6 | 1.18 |
| | 31/08/2015 | 6.22 | 4.79 | 0.18 | 1.12 | 1.617 | 56.6 | 65.1 | 1.70 |
| | 27/10/2015 | 6.32 | 4.61 | 0.22 | 1.24 | 1.72 | 88.0 | 65.9 | 1.33 |
| Chanson et al. [5] | 10/09/2010 | 6.03 | 4.49 | 0.33 | 1.77 | 2.27 | 105.7 | 75.4 | 1.30 |
| | 11/09/2010 | 5.89 | 4.20 | 0.30 | 1.81 | 2.27 | 108.8 | 75.8 | 1.20 |
| Reungoat et al. [30] | 07/06/2012 | 5.68 | 3.85 | 0.68 | 2.72 | 2.17 | 158.9 | 79.0 | 1.02 |
| Reungoat et al. [31] | 19/10/2013 | 6.09 | 4.32 | 0.29 | 2.05 | 2.35 | 85.6 | 65.0 | 1.27 |

Comparison between 2010, 2012, 2013 and 2015 flow conditions

Tidal range measured at Bordeaux port, 8.4 km upstream of sampling location; U: tidal bore celerity at sampling site; $V_1$: initial flow velocity on channel centreline; $d_1$: initial water depth at survey staff; $d_2$: conjugate water depth measured immediately after tidal bore passage at survey staff; $A_1$: initial cross-section area immediately prior to the tidal bore; $B_1$: initial free-surface width immediately prior to the tidal bore; $Fr_1$: tidal Froude number: $Fr_1 = (U + V_1)/(g \times A_1/B_1)^{1/2}$

The accuracy of the water elevation was 0.5 cm prior to the tidal bore and 1 cm during the tidal bore passage. The accuracy on the ADV velocity measurements was 1% of the velocity range (± 2.5 m/s) [24]. The error on the suspended sediment concentration (SSC) estimate was less than 5%.

## 2.2 Turbulent event analyses

A turbulent event may be defined as a series of turbulent fluctuations that contain more energy than the average turbulent fluctuations within a studied data section. The detection of turbulence bursting events was herein based upon the technique of Narasimha et al. [20], since it was found to be a more robust method applicable to point velocity signal time-series, including in unsteady rapidly-varied tidal bore flows. The method detects bursting events by comparing the absolute value of an instantaneous turbulent flux q (e.g. $q = v_x \times v_z$) with the standard deviation $q'$ of that flux over the data section. That is, a turbulent event occurs when:

$$|q| > k \times q' \tag{1}$$

where $|q|$ is the absolute value of the instantaneous flux q, k is a positive constant setting the threshold and $q'$ is the standard deviation of the flux. Narasimha et al. [20] and Trevethan and Chanson [35] conducted a sensitivity analysis on the threshold k. The outcomes yielded $k = 1$ which was selected herein.

In the present study, the turbulent momentum fluxes $v_x \times v_x$, $v_x \times v_y$ and $v_x \times v_z$, as well as turbulent sediment fluxes $ssc \times v_x$ and $ssc \times v_z$, were analysed. Here $v_x$, $v_y$, and $v_z$ are the longitudinal, transverse and vertical velocity component fluctuations, defined as $v_i = V_i - \overline{V_i}$ with $i = x, y, z$, and ssc is the suspended sediment concentration fluctuation defined as: $ssc = SSC - \overline{SSC}$, with $\overline{V_i}$ and $\overline{SSC}$ being the low-pass filtered velocity component and suspended sediment concentration respectively, x the longitudinal coordinate positive downstream, y the transverse coordinate positive towards the left bank (Fig. 2a, Right) and z the vertical coordinate positive upwards. The low-pass filtering derived based upon a sensitivity analysis conducted between an upper limit of the filtered signal and a lower limit corresponding to a period of about 0.8–1.0 s of the bore undulations [32]. The results yielded an optimum threshold of $f_{cutoff} = 2$ Hz, and the filtering was applied to all velocity components. In previous studies of undular bores [4, 5, 16, 30], a similar cutoff period $1/f_{cutoff}$ was selected, between the undulation period and half the undulation period of the tidal bore.

The standard deviation of the flux $q'$ was calculated as:

$$q' = \overline{(q - \overline{q})^2}^{1/2} \tag{2}$$

where each overbar denotes a low-pass filtering process.

For each data set, the information of each detected event was summarised. Figure 3 presents some example and introduces a number of basic definitions. Figure 3a shows four isolated events and Fig. 3b illustrates two isolated flux events. The event duration $\tau$ is the time interval between the zeroes in momentum flux (e.g. $q = v_x \times v_z = 0$), nearest to the sequence of data points satisfying Eq. (1). The dimensionless amplitude A of an event is the ratio of the averaged flux amplitude during the event to the long-term mean flux of the entire data section:

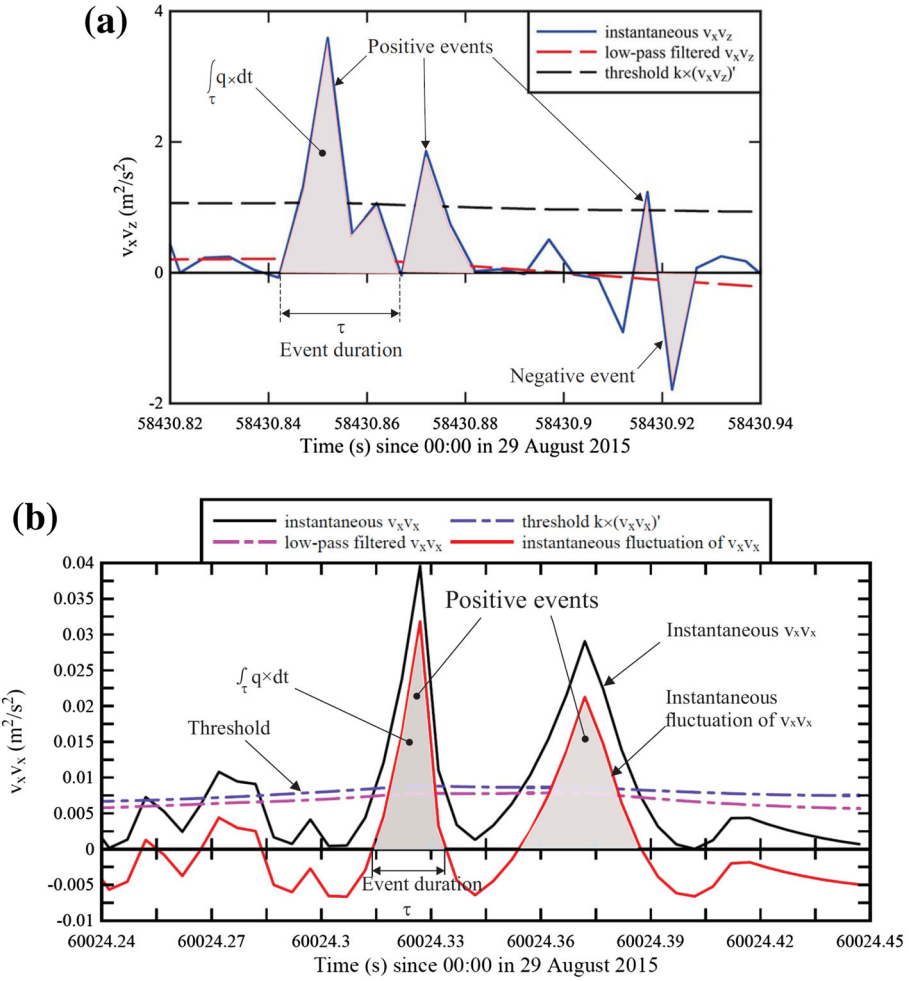


**Fig. 3** Momentum flux data collected on 29 August 2015 and turbulent flux event definitions. **a** Momentum flux $v_x \times v_z$, **b** momentum flux $v_x \times v_x$

$$A = \frac{1}{\tau} \times \int_{\tau} \frac{q}{\overline{q}} \times dt \tag{3}$$

where $\overline{q}$ is the low-pass filtered component of the flux fluctuation and $dt = 1/f_{scan}$ ($f_{scan} = 200$ Hz). The relative contribution of an event to the total momentum flux of the data section is called the relative magnitude m defined as:

$$m = \frac{A \times \tau}{T} \tag{4}$$

where T is the duration of the data set. The dimensionless event magnitude was calculated based upon Eq. (4), with the calculation duration T equals to 0.5 s: that is, the inverse of the cut-off frequency used in the low-pass filtering process.

## 3 Observations

### 3.1 Presentation

On 29 and 31 August, and 27 October 2015, the tidal bore formed at the downstream end of the Arcins channel. The bore extended rapidly across the entire channel width. The tidal bore was basically undular, although the bore was breaking for a few metres next to the left bank, as seen in Fig. 2b. At the sampling location, all the bores are undular, owing to the relatively deep water. Although the bore was undular, the free-surface elevation rose very rapidly during the bore passage: i.e., by 0.3–0.5 m in the first 10–15 s, as illustrated in Figs. 2b and 4. The bore propagated upstream for the entire length of the Arcins channel. At the sampling site, the bore front passage was followed by a few well-formed free-surface undulations, then some disorganised wave motion, and later some stronger whelps. These strong whelps were observed 60–200 s after the bore front, with a characteristic wave period of about 1 s ± 0.5 s. They are seen in Fig. 4d for $t > 56{,}280$ s.

The bore shape was characterised its Froude number defined as $Fr_1 = (V_1 + U)/(g \times A_1/B_1)^{0.5}$ [3], where $V_1$ is the initial flow velocity positive downstream, U is the bore celerity positive upstream, g is the gravity acceleration, $A_1$ is the initial flow cross-section area and $B_1$ is the initial free-surface width, which were derived from bathymetric surveys conducted daily. The bathymetric surveys were conducted manually, typically 1 h before bore passage. These flow properties are summarised in Table 1, as well as the initial and conjugate water depth readings on the survey staff. Basically the Froude number ranged from 1.2 to 1.7, consistent with the undular nature of the bore except on 31 August 2015. On 31 August 2015, the bore front was undular on the channel centreline and towards to the right bank, but breaking very close to the left bank in the shallower waters.

Overall, the results of each day were similar, in the context of Fig. 4. The tidal bore flow patterns were consistent with past field observations between 2010 and 2013, albeit there were differences in terms of freshwater conditions, in bathymetric conditions associated with siltation and scour, and in tidal conditions between each tidal bore event (Table 1). Table 1 illustrates differences in terms of the tidal range (column 3), bore celerity (column 4), initial depth (column 6) and tidal bore Froude number (column 10) for the field studies conducted in 2010, 2012, 2013 and 2015.

### 3.2 Velocity measurements

Prior to the bore, during the end of ebb tide, the current velocity decreased in the Arcins channel with time (Fig. 4 for $t < 56{,}238$ s). Immediately prior to the bore, the surface velocity dropped down to + 0.2–0.3 m/s at the channel centre. The tidal bore occurrence had a marked effect on the velocity field and water depth, as illustrated in Fig. 4 about $t > 56{,}238$ s. The passage of the tidal bore was associated with a very rapid rise of the water elevation, followed by free-surface undulations or secondary waves. The velocity measurements indicated consistently a very-rapid flow deceleration and quasi-sudden flow reversal during the bore passage, followed by large and rapid fluctuations of all velocity components during the early flood tide. The maximum flow deceleration ranged from − 0.65 to less than − 1.4 m/s$^2$ (Appendix 1). Appendix 1 summarises a number of velocity properties prior to, during and after the bore passage for all three field data sets, as well as for the 2012 and 2013 studies. Figure 4 presents a complete data set, with Fig. 4d showing details of tidal bore passage.

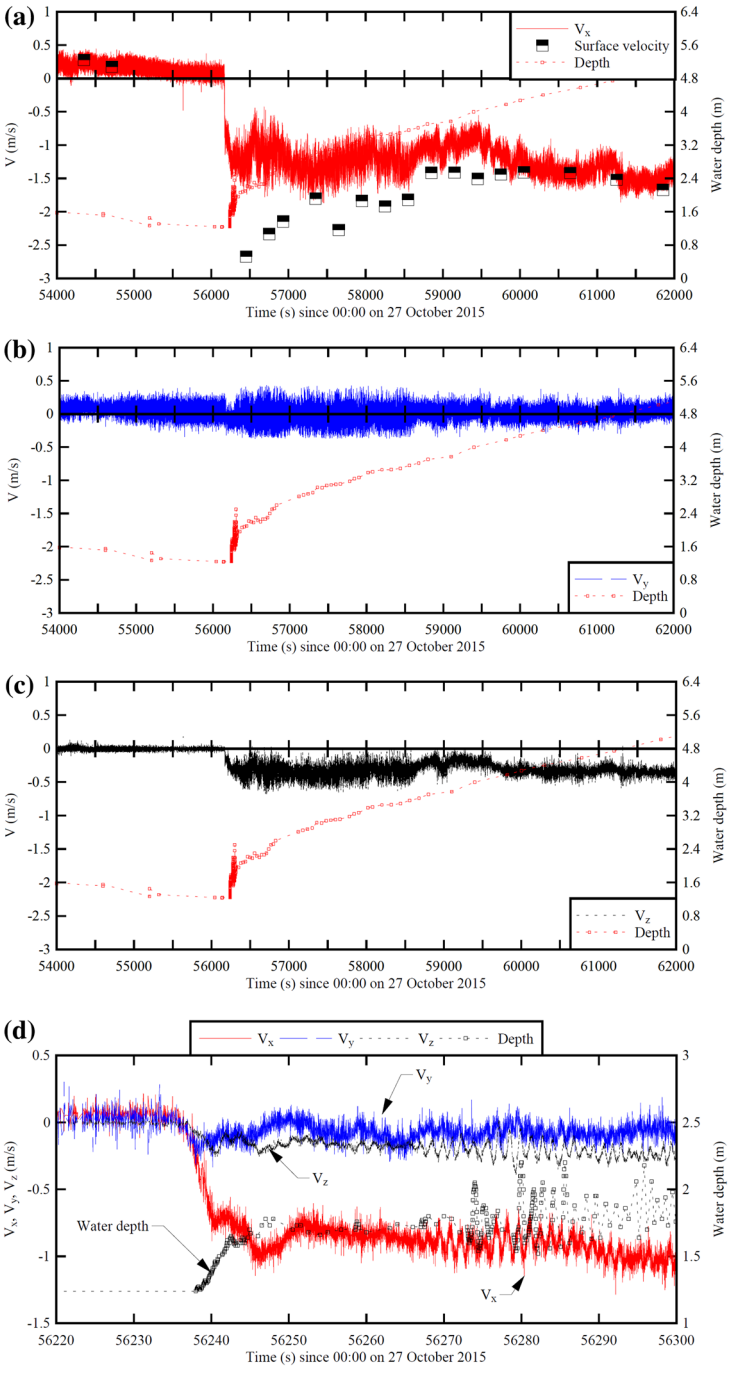


**Fig. 4** Time-variation of free-surface elevation and instantaneous velocity components during the tidal bore of the Garonne River (France) on 27 October 2015. **a** Longitudinal velocity component $V_x$, **b** transverse velocity component $V_y$, **c** vertical velocity component $V_z$, **d** details about tidal bore passage

The bore passage was associated with large fluctuations of all velocity components, lasting throughout the flood tide (Fig. 4). The flood flow was very energetic. Large velocity fluctuations were recorded for the first 2 h following the bore. For example, the dimensionless velocity fluctuations $v'/|\overline{V_x}|$ ranged from 8 to 10% 1 h after the bore passage (Appendix 1). The horizontal turbulence ratio $v'_y/v'_x$ was between 0.51 and 0.85, with the vertical turbulence ratio $v'_z/v'_x$ being between 0.35 and 0.52. Such values were comparable to laboratory observations in straight prismatic rectangular channels [21, 22]. Overall $v'_z/v'_x$ was about two-thirds of the horizontal turbulence intensity $v'_y/v'_x$, and such a finding indicated some turbulence anisotropy during the flood tide motion.

### 3.3 Turbulent shear stresses

The turbulent Reynolds stress tensor was calculated as the product of velocity fluctuations times the water density. The effect of suspended sediment load on fluid density was ignored. The turbulent velocity fluctuations v were calculated as: $v = V - \overline{V}$, where $\overline{V}$ is the low-pass filtered velocity component [4, 27, 31]. Typical data are shown in Fig. 5. The complete data sets are presented in Reungoat et al. [32]. The field data indicated large turbulent shear stresses, together with large and rapid fluctuations, during the passage of and the early flood tidal flow after the tidal bore, for all Reynolds stress tensor components. The measurements yielded significantly larger turbulent shear stress levels after the tidal bore passage, compared to before the bore. All the data highlighted large magnitudes of instantaneous shear stresses after the bore passage (Fig. 5). This is illustrated in Fig. 5, presenting the time-variations of four turbulent Reynolds stress components during a field study. All graphs showed large turbulent stresses for the first 1000 s following the bore passage, with maximum and mean Reynolds stress magnitudes being two to ten times larger after the bore passage than during the late ebb tide.

For the present data set, maximum instantaneous normal shear stress amplitudes in excess of 150 Pa were recorded shortly after the tidal bore, and maximum instantaneous tangential stress magnitude up to more than 100 Pa. Quantitatively as well as qualitatively, the data were comparable to earlier tidal bore field data [5, 30, 31].

### 3.4 Spectral analyses

Power spectrum analyses were conducted in terms of the longitudinal velocity component, turbulent kinetic energy (TKE), and normal and tangential Reynolds stresses during the late ebb tide and very early flood tide, for the tidal bore events, as suggested by the reviewer. The results were consistent for all events. Figure 6 presents typical results for the tidal bore event on 29 August 2015, where $T_{bore}$ is the time of passage of the tidal bore. The late ebb and flood tide calculations were performed over 1000 s, and the early flood tide calculations were conducted over 100 s only, owing to the very-rapidly changing flow conditions.

The velocity fluctuation spectra were compared to the $-1$ slope for the overlap region [23, 26] and $-5/3$ slope, i.e. Kolmogorov cascade in the inertial sub-range [33] (Fig. 6a). Herein the ADV control volume was outside of the wall region and the velocity spectra tended to follow the $-1$ slope during the late ebb tide. Note the level-off of spectral density functions at high frequency caused by the white Doppler noise, an intrinsic part of all Doppler-based backscatter systems [17]. The data indicate that the horizontal velocity component data are biased because of the Doppler noise from above 30–40 Hz. The

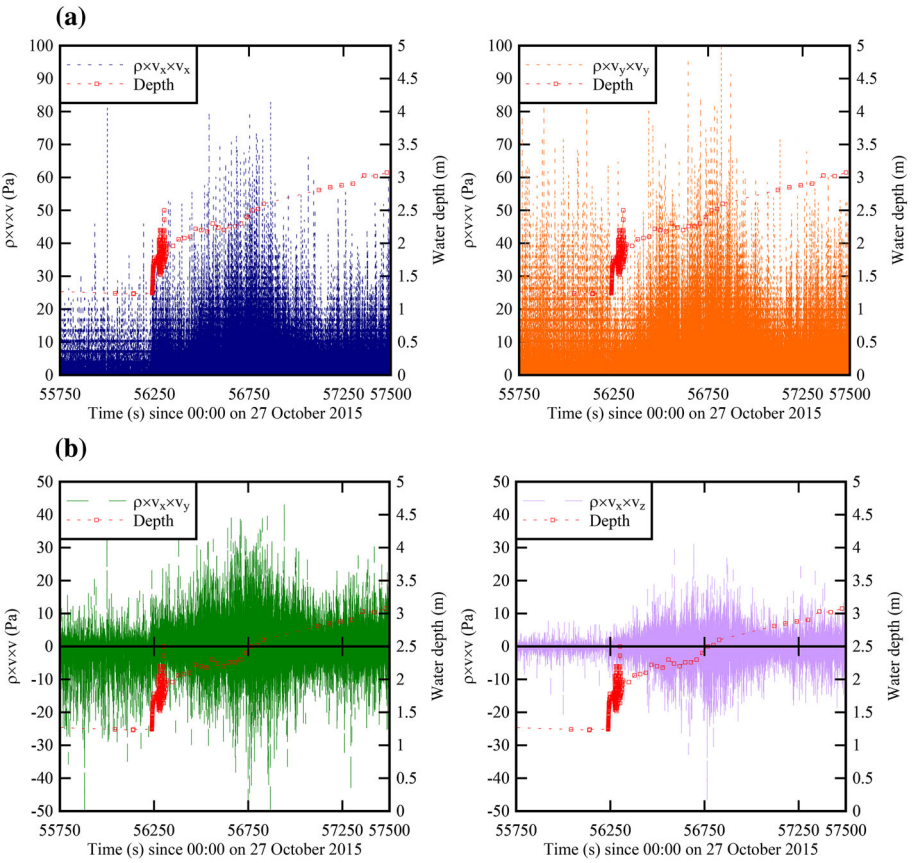


**Fig. 5** Time-variations of instantaneous Reynolds stresses and water depth in the Arcins channel on 27 October 2015. **a** Normal stresses $\rho \times v_x \times v_x$ and $\rho \times v_y \times v_y$, **b** tangential stresses $\rho \times v_x \times v_y$ and $\rho \times v_x \times v_z$

overlap region was marked by the existence of a $-1$ slope in the power spectra shown in Fig. 6a. The very early-flood tide data presented showed a different shape, with lesser energy at high frequency, possibly linked to the production of large-scale turbulence, clearly evidenced by large surface scars during the bore passage. The flood tide data presented systematically a different pattern, with a $-1$ slope up to 10–20 Hz, a $-5/3$ slope between 10–20 and 50–60 Hz, and $-11$ slope above 60 Hz. The latter might be the result of combined effects of turbulence-free-surface interactions and acoustic backscatter signal attenuation in high suspended sediment concentrations. More generally all the spectral analyses showed marked differences for the very-early flood tide results (Fig. 6).

## 4 Unsteady turbulent flux event results

The normalised probability density functions (PDFs) of turbulent event duration and amplitude were analysed for the entire sampling duration on each day. Typical results for $v_x \times v_z$ are shown in Fig. 7 and a statistical summary is presented in Appendix 2. Note

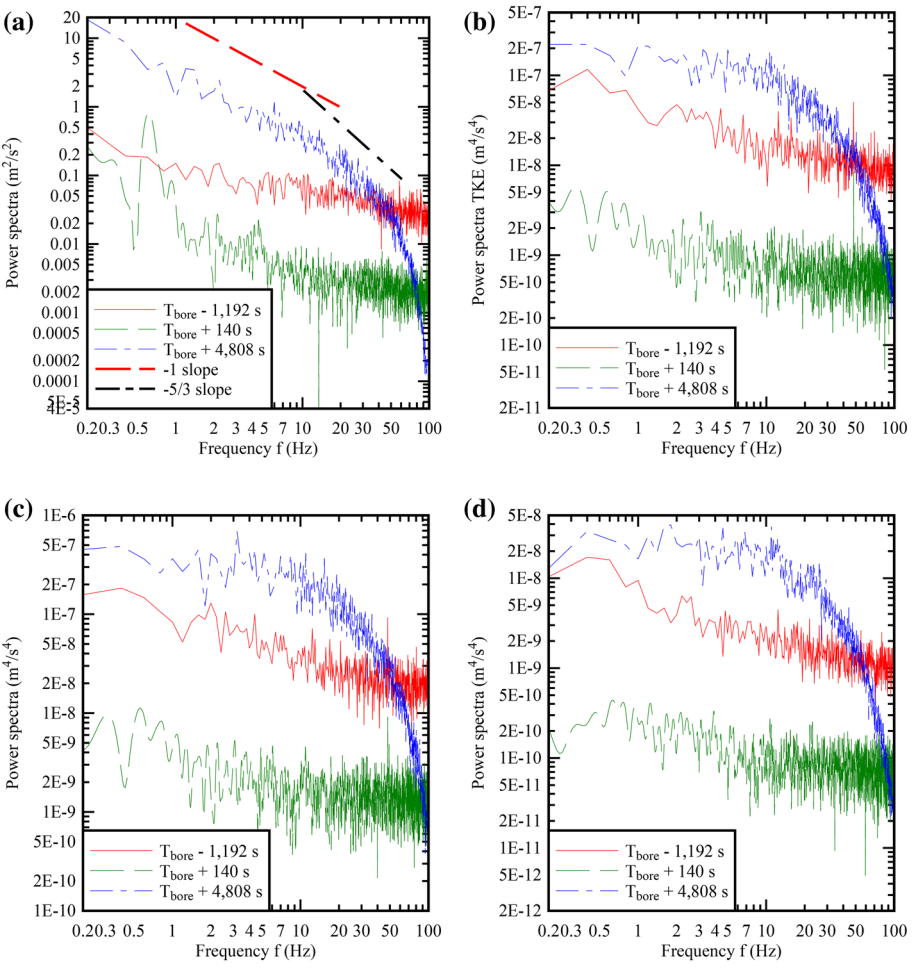


**Fig. 6** Spectral analyses of the longitudinal velocity component, turbulent kinetic energy TKE = $0.5 \times (v_x^2 + v_y^2 + v_z^2)$, normal Reynolds stress $v_x^2$ and tangential Reynolds stress $v_x v_z$ during the late ebb tide, very early flood tide and flood tide on 29 August 2015. **a** Longitudinal velocity component, **b** turbulent kinetic energy, **c** normal stress $v_x^2$, **d** tangential stress $v_x v_z$

that, in Fig. 7a, the event duration PDF data are shown with logarithmic scales for both axes.

Overall the results highlighted a skewed distribution of event duration with a well-defined mode, for all fluxes measured on 29 and 31 August and 27 October 2015. The event duration ranged from 0.002 to 2.5 s, with some extreme events lasting more than 2 s, albeit representing less than $3 \times 10^{-4}$ %. It is acknowledged that the low-pass filtering cut-off frequency of 2 Hz might influence the upper range of data. The majority of the events ($\sim$ 60%) lasted less than 0.02 s, with 0.2% of events having a duration longer than 0.1 s. The normalised PDF of event duration showed a monotonic decrease with increasing event duration between 0.04 and 0.3 s, which was best correlated by:

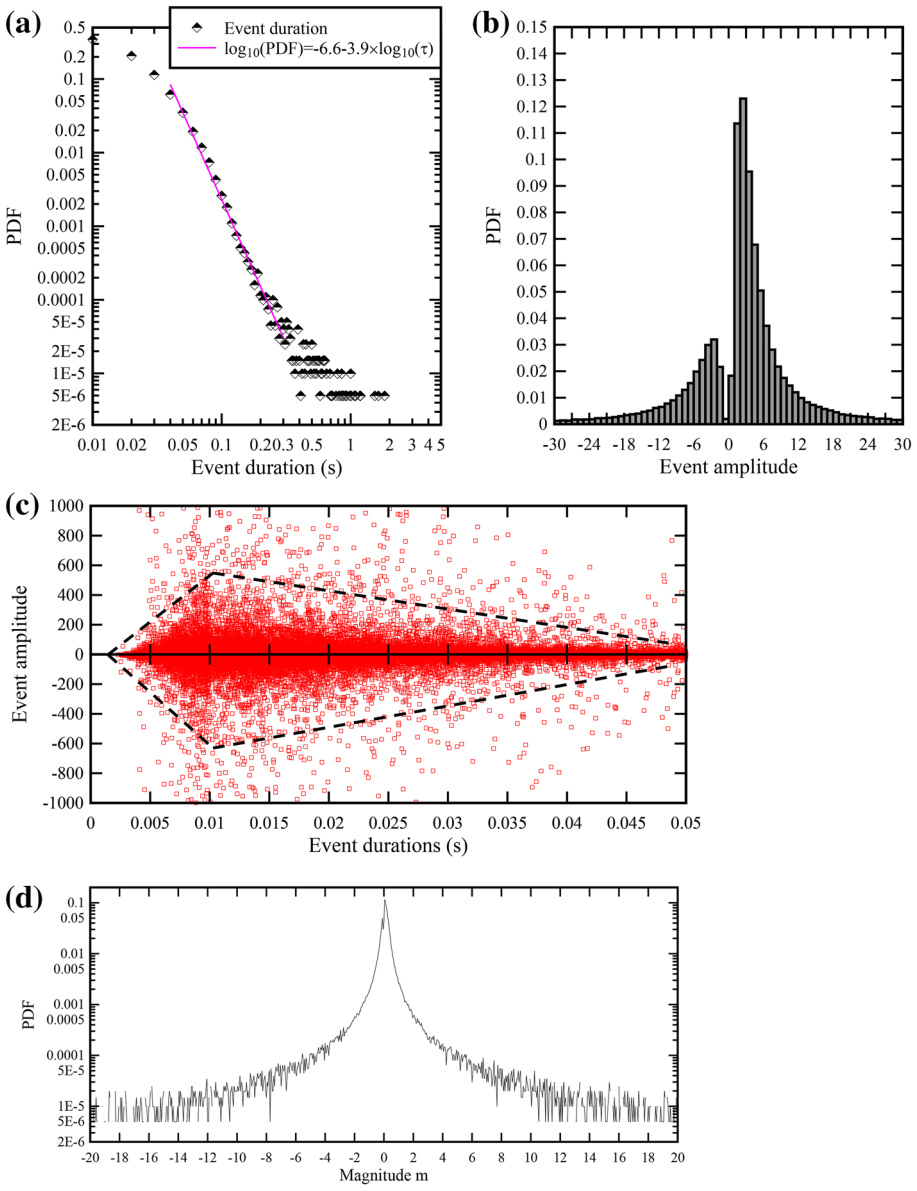


**Fig. 7** Event duration and amplitude for the momentum flux $v_x \times v_z$ in the Garonne River on 31 August 2015. **a** Normalised PDF of event duration τ, **b** normalised PDF of event amplitude A, **c** relationship between turbulent event amplitude A and duration τ—black dashed lines outline the envelop, **d** normalised PDF of dimensionless event magnitude m

$$\log_{10} \mathrm{PDF} = \mathrm{a} \times \log_{10} \tau + \mathrm{b} \quad 0.04\ \mathrm{s} < \tau < 0.3\ \mathrm{s} \tag{5}$$

where τ is the event duration, PDF is the probability density function, a and b are constants, with a varying between −6 to −8 and b between −3.5 to −4.5. This data trend [Eq. (5)] was observed consistently for the entire data sets on 29, 31 August and 27 October.

The event amplitude for the entire data set showed a bi-modal distribution for all flux data, except $v_x \times v_x$, with a mean value close to 0 (e.g. Fig. 7b). The first mode with probability of 6–10% was associated with positive event amplitudes ranging from 2 to 3. The second mode was associated with negative event amplitudes between $-2$ and $-3$, and a probability about 3–4%. The event amplitude $v_x \times v_x$ PDF was mono-modal. The event amplitude data showed that the majority of the events were associated with positive amplitudes for all fluxes, albeit, negative events and positive events had amplitude magnitude of the same order of magnitude.

The relationship between event amplitude and duration presented a characteristic envelop shape. For all flux data collected on the 3 days, the event duration ranged from 0.002 to 2.5 s, and the event amplitude ranged from $-1\times10^7$ to $1\times10^7$. The relationship between event amplitude and duration showed a diamond-like envelop shape, symmetrical about the horizontal axis (event duration) for the majority (over 99.8%) of all flux data (Fig. 7c). The event amplitude magnitude range increased with event duration for $\tau < 0.01$ s. For $\tau > 0.01$ s, the event amplitude magnitude range decreased with increasing event duration. The results implied maximum event amplitudes associated with event durations of approximately 0.01 s. Extremely long events, with over 2 s duration, were associated with small amplitude magnitude between 0 and 10. The symmetrical shape of the data sets indicated an equal percentage of positive and negative events. Figure 7c shows typical results in terms the momentum flux $v_x \times v_z$, for all events detected throughout the sampling duration on 31 August 2015. Figure 7c presents the relationship between event amplitude and duration for the tangential stress $v_x v_z$. For the 3 h long data set, more than 200,000 turbulent events were detected and plotted in Fig. 7c.

The dimensionless event magnitude was calculated based upon Eq. (4), with the calculation duration T equals to 0.5 s: that is, $T = 1/f_{cutoff}$. Figure 7d shows a typical probability density function of event magnitude for fluxes $v_x \times v_z$ measured on 31 August 2015. Overall, the PDF of event magnitude showed log-normal distributions for all fluxes. The majority of events (over 95.5%) were associated with a dimensionless magnitude range of $-2$ to 2, for all fluxes measured on all days. The shape of the PDF compared well past field studies in natural systems [20, 35], albeit with a much wider magnitude range with high probability herein. The present study also showed two modes, one positive and on negative, with the negative mode having a lower probability density (Fig. 7d). This was consistent with the PDF for event amplitude (Fig. 7b).

Since the propagation of tidal bore in a natural river is a highly unsteady and turbulent process, the time-variations of turbulent event duration and amplitude were analysed with respect to the time-variations of the free-surface elevation and bore passage. Typical results were presented in Fig. 8, in which the event duration are compared to water depth, SSC, suspended sediment flux and Reynolds stress data. For all momentum and suspended sediment fluxes, large fluctuations in event amplitude and durations were observed throughout the entire sampling duration. For the data collected on 29 and 31 August 2015, the event duration for all fluxes showed an abrupt peak with values in excess of 2 s shortly after the bore passage (Fig. 8). No obvious peak in duration was observed in the measurements for 27 October 2017. Such extremely long events were associated with comparatively small magnitude of amplitude: i.e., less than 1.

As observed in Fig. 8, the peak in event duration seemed to be associated with the rapid increase of suspended sediment concentration and rapid increase in the suspended sediment flux magnitude, shortly after the bore passage ($\sim$ 100–400 s). A previous study suggested a two-stage bed erosion process during the tidal bore propagation, corresponding to an initial surface erosion, followed some delayed bulk mass erosion [14]. In Fig. 8, these two

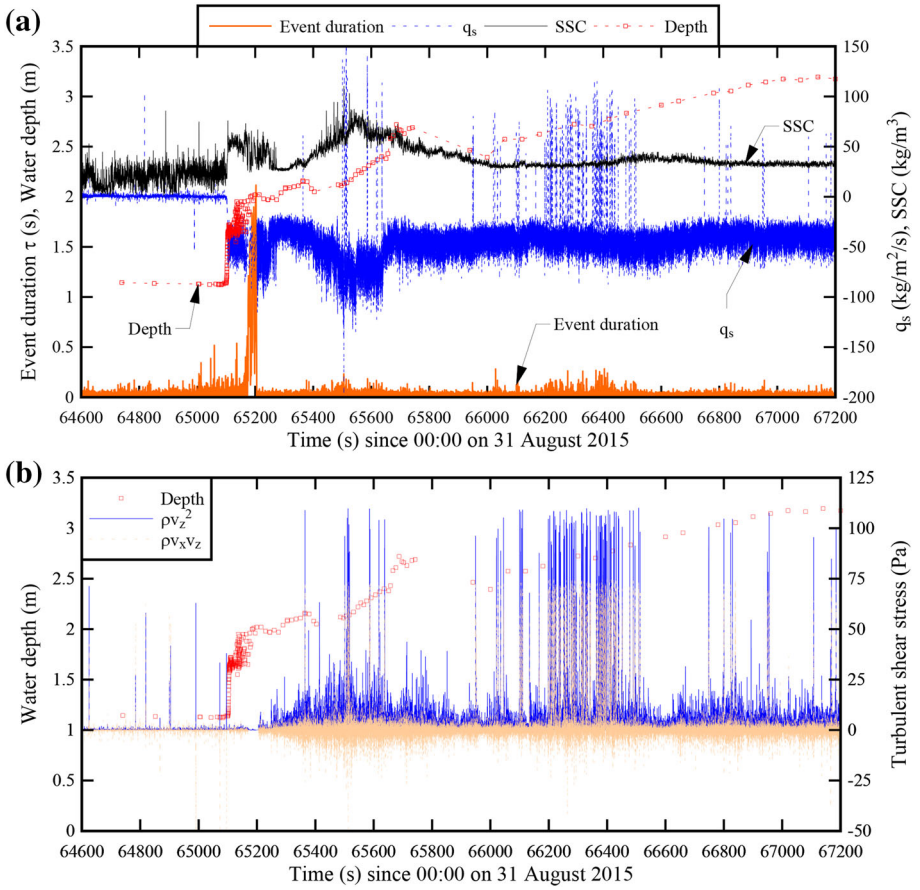


**Fig. 8** Time variation of instantaneous event duration of suspended sediment flux $v_x \times$ ssc on 31 August 2015—comparison with water depth, Reynolds stresses $\rho \times v_z^2$ and $\rho \times v_x \times v_z$, low-pass filtered suspended sediment concentration SSC, and suspended sediment flux per unit area $q_s = Vx \times SSC$. **a** Instantaneous event duration of suspended sediment flux $v_x \times$ ssc, water depth, low-pass filtered SSC (solid black line), suspended sediment flux per unit area $q_s = Vx \times SSC$ (dashed blue line), **b** instantaneous water depth, and Reynolds stresses $\rho \times v_z^2$ (thin green line) and $\rho \times v_x \times v_z$ (dashed beige line)

stages are clearly marked by the consecutive negative peaks in the suspended sediment flux data and positive peaks in the low-pass filtered SSC data, shortly after the bore passage: i.e., t ~ 65,200 s and t ~ 65,500 s (Fig. 8). On 29 August 2016, the maximum event duration was associated with the second stage of erosion, whereas the maximum event duration on 31 August was associated with the first stage of erosion. Overall, the data suggested the possibility of long-lasting turbulent events occurring simultaneously with sediment erosion processes during tidal bore passage.

Statistical properties were calculated for three distinct phases of the flow motion: the initial flow phase (i.e. late ebb flow) defined as the flow period immediately prior to the bore arrival, the very early flood tide phase defined as the highly-unsteady rapid-varied flow period about 20 s after the bore passage, and the flood tide phase defined as the gradually-varying flow period about 1 h after the tidal bore passage. A detailed summary of time-average statistics are presented in Appendix 2, for different phases throughout a

full sampling duration. In Appendix 2, Tables 3 and 4 regroup the complete datasets on 29, 31 August and 27 October.

The turbulent event statistics showed a similar number of events for all fluxes throughout the entire sampling duration: i.e., before, during and after the bore passage. For all fluxes, the median event durations were of the same order of magnitude: i.e., $\tau \approx 0.01$–$0.03$ s. The very-early flood tide phase was associated with slightly longer event durations for all fluxes, while the late ebb flow and flood tide motion were associated with events of about similar average duration. Compared to previous field studies, the median event duration was herein smaller, even during the very-early flood tide phase of the tidal bore. In a micro-tidal estuary, Trevethan and Chanson [35] reported an average dimensionless event duration: $\tau \times \left|\overline{V_x}\right|/d \approx 0.07$, while Narasimha et al. [20] obtained $\tau \times \overline{V_x}/\delta \approx 0.02$ in an atmospheric boundary layer, with $\delta$ the boundary layer thickness. Laboratory observations of dye concentration bursting events in a laboratory open flume yielded dimensionless burst durations between 0.06 and 0.07 [28]. The dimensionless event duration in the present study was two to three orders of magnitude shorter, namely between $10^{-5}$ and $10^{-4}$. In the Garonne River, the very short event duration revealed the highly fluctuating nature of the flow and the bursting characteristics of the turbulent events associated with tidal bore propagation.

The time series of turbulent event amplitude showed large fluctuations of all fluxes. The standard deviation of event amplitude for all fluxes ranged from 500 to 20,000, regardless of the flow phase: it was several orders of magnitude higher than the median value. The median amplitude for all fluxes and all flow phases were between 2 and 5, with the initial and flood tide phase typically associated with higher median amplitude. In comparison to the data of Trevethan and Chanson [35], the present study documented median event amplitudes of the same order of magnitude, but the standard deviation of the event amplitude detected in the present study was two orders of magnitudes larger than that of Trevethan and Chanson [35] for most momentum fluxes.

Further investigations were conducted into the probability density function of event duration and amplitude for fluxes during different flow phases (initial flow, very early flood tide and flood tide). Figure 9 show event duration (Left) and amplitude (Right) data for momentum flux $v_x \times v_z$ on 31 August 2015. In Fig. 9, the normalised probability density functions of event duration during the late ebb and flood tide phases were very similar, and comparable to results presented in Fig. 7a. In contrast, the PDF of event duration during the very early flood tide phase showed a number of differences (Fig. 9b, Left). Namely larger probabilities ($\sim 4\%$) were observed corresponding to longer event durations (greater than 0.2 s) immediately after the tidal bore passage. The relationship between probability and event duration followed Eq. (5), albeit for a much shorter range of event duration ($0.03\text{ s} < \tau < 0.1$ s), with a smaller gradient coefficient a.

The normalised probability density functions of event amplitudes showed self-similar shapes during the three flow periods (Fig. 9). The results were consistent on each day for the entire sampling duration (Fig. 7b). For all three flow phases, the majority of event amplitudes were positive, with a larger ratio of positive to negative event number during the initial flow phase (Fig. 9a). The very early flood tide phase was associated with high probabilities of large amplitude magnitudes, especially negative event amplitudes. The flood tide phase showed similar shape of probability distribution as observed in the initial flow phase, but with a much smaller ratio between the proportion of positive and negative events.

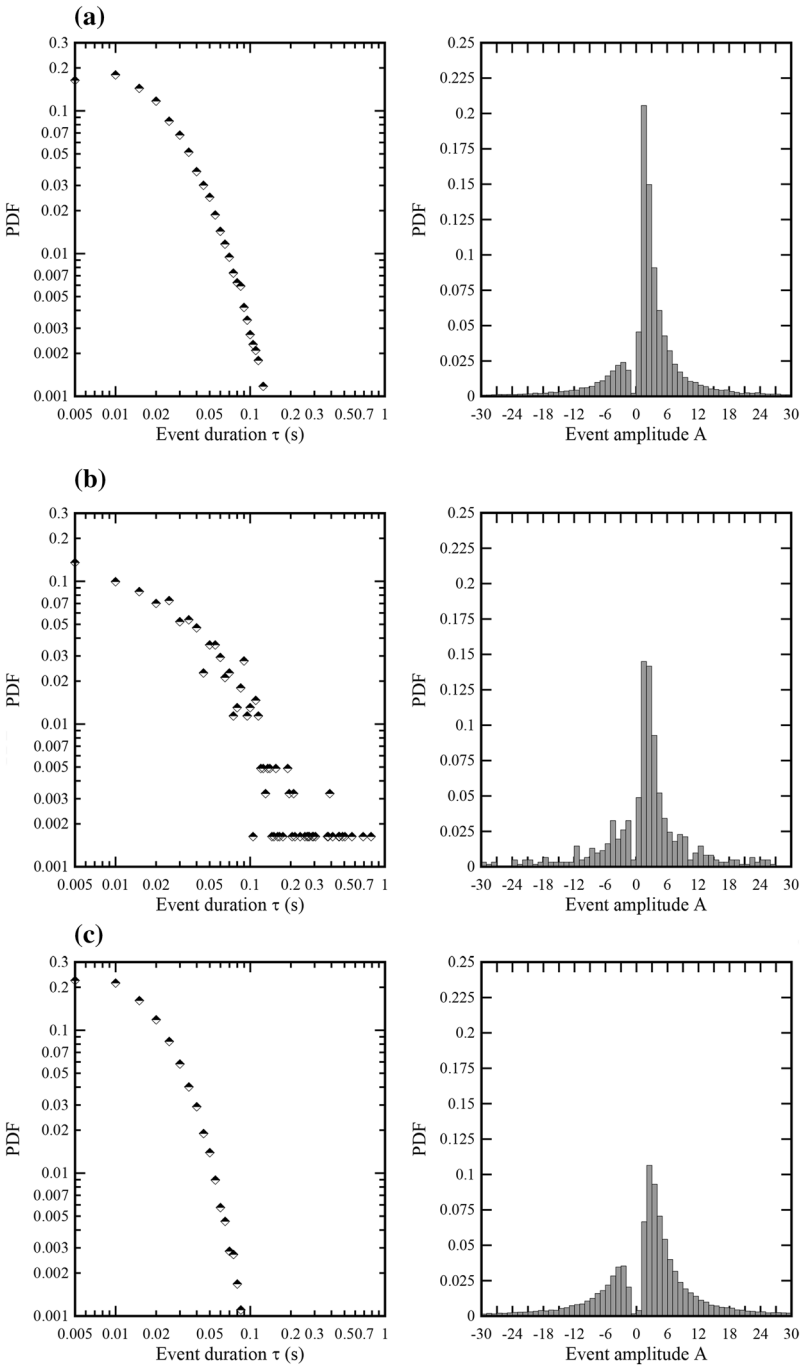


**Fig. 9** Normalised probability density functions of event duration t (Right) and event amplitude A (Left) for the momentum flux $v_x \times v_z$ during the late ebb tide flow, very early flood tide and flood tide phases on 31 August 2015. **a** End of ebb tide, **b** very early flood tide immediately after tidal bore passage, **c** flood tide (1 h after tidal bore passage)

## 5 Conclusion

The occurrence of tidal bores has a significant impact on natural estuarine systems, and the bore propagation is associated with intense sediment suspension concentrations and fluxes. The tidal bore of the Garonne River was investigated in the Arcins channel on 29 August, 31 August and 27 October 2015. Instantaneous velocity measurements were performed continuously at high-frequency (200 Hz) without interruption prior to, during and after each afternoon tidal bore. The tidal bore occurrence had a marked effect on the velocity field, including a rapid flow deceleration and flow reversal during the bore passage. The turbulent Reynolds stress data indicated large shear stresses, together with large and rapid fluctuations, during the bore passage and the early flood tide.

A turbulent event analysis was developed for and applied to in the highly-unsteady rapidly-varied tidal bore flow. The analysis was based upon basic concepts, in which turbulent bursting events were defined in terms of the instantaneous turbulent flux, and the method was tested for the rapidly-varied, highly-unsteady tidal bore flood flow motion. The turbulent event data showed relatively close results for all studies and all fluxes: (a) a very-large majority of turbulent events had a duration less than 0.01 s; (b) there were on average 20 turbulent events per second; (c) for all studies, the event duration showed some tidal trend, with longer turbulent events immediately after the tidal bore passage, occurring simultaneously with major sediment erosion processes; (d) all data suggested the occurrence of long-lasting turbulent events almost simultaneously with sediment erosion processes during the bore passage; and (e) a comparison between present data and past field studies in micro-tidal estuary and atmospheric boundary layer showed herein shorter dimensionless event durations, larger event amplitudes and magnitudes.

Altogether the present analysis suggested that the proposed turbulent event analysis may be applicable to rapidly-varied tidal bore flow. It provides quantitative details into the turbulent bursts that are responsible for major mixing and sedimentary processes. While the turbulent event analysis was expanded for and applied to undular tidal bores, it is believed that the method is valid for both breaking and undular bores, and more generally for highly-unsteady turbulent geophysical flows.

**Acknowledgements** The authors acknowledge the assistance of Patrice Benghiati and the permission to access and use the pontoon in the Bras d'Arcins. They thank all the people who participated to the field works, and without whom the study could not have been conducted. The authors thank Dr. Frédérique Larrarte (IFSTTAR Nantes, France), Professor Michele Mossa (Politecnico di Bari, Italy), Dr. Kyle Strom (Virginia Tech, USA), and Dr. Emmanuel Mignot (INSA Lyon, France) for some initial comments. They also thank Professor Pierre Lubin (University of Bordeaux, France) for a number of useful discussions and inputs.

**Funding** The authors acknowledge the financial assistance of the Agence Nationale de la Recherche (Projet Mascaret ANR-10-BLAN-0911). They further thank all the field work participants for their assistance and hard work on site.

## Appendix 1: Velocity characteristics about the tidal bore passage

See Table 2.

**Table 2** Velocity properties immediately prior to, during and immediately after the tidal bore in 2015

| Flow properties | Date | | | | |
|---|---|---|---|---|---|
| | 7/6/12 | 19/10/13 | 29/8/15 | 31/8/15 | 27/10/15 |
| Froude number $Fr_1$ | 1.02 | 1.27 | 1.18 | 1.70 | 1.33 |
| Initial flow conditions | | | | | |
| Initial water depth (m)[a] | 2.72 | 2.05 | 1.685 | 1.12 | 1.24 |
| Initial surface velocity (m/s)[b] | + 0.68 | + 0.255 | + 0.29 | + 0.18 | + 0.22 |
| Initial velocity $\overline{V_x}$ (m/s)[c] | + 0.34 | + 0.106 | + 0.094 | + 0.005 | + 0.066 |
| Bore passage | | | | | |
| Maximum deceleration $(\partial\overline{V_x}/\partial t)_{max}$ (m/s$^2$)[c] | − 0.619 | − 0.504 | *− 1.2* | − 0.883 | − 0.645 |
| Very early flood tide ($T_{bore}$ + 20 s) | | | | | |
| $\overline{V_x}$ (m/s)[c] | − 0.47 | − 0.83 | − 0.82 | − 0.83 | − 0.81 |
| $\overline{V_y}$ (m/s) | + 0.12 | − 0.04 | + 0.02 | − 0.06 | − 0.06 |
| $\overline{V_z}$ (m/s) | − 0.02 | − 0.13 | − 0.11 | − 0.20 | − 0.16 |
| $v'_x$ (m/s) | 0.049 | 0.040 | 0.085 | 0.047 | 0.054 |
| $v'_y$ (m/s) | 0.026 | 0.040 | 0.046 | 0.070 | 0.058 |
| $v'_z$ (m/s) | 0.051 | 0.025 | 0.026 | 0.031 | 0.026 |
| Early flood tide wave motion | | | | | |
| Time after bore passage (s)[c] | – | 40 | 180 | 170 | 50 |
| Velocity amplitude $V_x$ (m/s) | – | 0.13 | 0.165 | 0.138 | 0.175 |
| Velocity amplitude $V_x$ (m/s) | – | 0.075 | 0.10 | 0.102 | 0.10 |
| Velocity oscillation period (s) | – | 1.55 | 1.5 | 1.47 | 1.33 |
| Backward bore (± 100 s) | | | | | |
| Time after bore passage (s) | – | 632 | – | 568 | 583 |
| $\overline{V_x}$ (m/s)[c] | – | − 0.87 | – | − 1.06 | − 1.10 |
| $v'_x$ (m/s) | – | 0.397 | – | 0.219 | 0.177 |
| $v'_y$ (m/s) | – | 0.097 | – | 0.138 | 0.126 |
| $v'_z$ (m/s) | – | 0.064 | – | 0.120 | 0.096 |
| Flood tide ($T_{bore}$ + 3600 s) | | | | | |
| $\overline{V_x}$ (m/s)[c] | – | − 1.16 | − 0.91 | − 1.27 | − 1.20 |
| $v'_x$ (m/s) | – | 0.077 | 0.088 | 0.116 | 0.116 |
| $v'_y$ (m/s) | – | 0.049 | 0.074 | 0.061 | 0.059 |
| $v'_z$ (m/s) | – | 0.029 | 0.044 | 0.060 | 0.041 |

Comparison with 2012 and 2013 observations

[a]At survey staff

[b]At channel centre

[c]ADV data; *Italic data*: suspicious data

## Appendix 2: Statistical properties of turbulent events

See Tables 3 and 4.

**Table 3** Statistical properties of turbulent events during the late ebb tide flow, very early flood tide and flood tide phases on 29, 31 August and 27 October 2015 for the momentum fluxes $v_x \times v_z$ and $v_x \times v_y$ and suspended sediment concentration flux $v_z \times$ ssc and $v_x \times$ ssc

| Date | 29/08/2015 | | | | 31/08/2015 | | | | 27/10/2015 | | | |
|---|---|---|---|---|---|---|---|---|---|---|---|---|
| Total sampling duration (s) | 13,583 | | | | 10,835 | | | | 9861 | | | |
| Initial water depth (m) | 1.685 | | | | 1.12 | | | | 1.24 | | | |
| Tidal bore Froude number $Fr_1$ | 1.18 | | | | 1.7 | | | | 1.33 | | | |
| | $v_xv_z$ | $v_xv_y$ | $v_z \times$ ssc | $v_x \times$ ssc | $v_xv_z$ | $v_xv_y$ | $v_z \times$ ssc | $v_x \times$ ssc | $v_xv_z$ | $v_xv_y$ | $v_z \times$ ssc | $v_x \times$ ssc |
| Total number of events | 242,917 | 280,855 | 308,464 | 322,778 | 201,619 | 268,921 | 271,955 | 283,966 | 214,386 | 240,216 | 239,628 | 246,582 |
| Initial flow conditions[a] | | | | | | | | | | | | |
| Median event amplitude | 2.7 | 2.84 | 4.24 | 4.37 | 2.29 | 3.88 | 4.26 | 4.36 | 2.29 | 2.11 | 3.48 | 3.22 |
| Standard deviation of event amplitude | 653.62 | 692.96 | 6405.65 | 16,522.63 | 2269.09 | 1893.42 | 3732.49 | 2256.61 | 245.98 | 581.89 | 533.41 | 283.97 |
| Median event duration (s) | 0.02 | 0.02 | 0.01 | 0.01 | 0.02 | 0.01 | 0.01 | 0.01 | 0.02 | 0.02 | 0.02 | 0.02 |
| Standard deviation of event duration | 0.02 | 0.01 | 0.01 | 0.01 | 0.02 | 0.01 | 0.01 | 0.01 | 0.02 | 0.02 | 0.02 | 0.02 |
| Very early flood tide ($T_{bore}$ + 20 s)[b] | | | | | | | | | | | | |
| Median event amplitude | 2.99 | 3.65 | 4.23 | 4.12 | 2.24 | 2.32 | 2.68 | 2.59 | 2.88 | 3.52 | 4.19 | 4.94 |
| Standard deviation of event amplitude | 2658.54 | 286.54 | 711.82 | 72.23 | 305.61 | 94.55 | 517.85 | 138.47 | 229.26 | 143.12 | 179.72 | 86.89 |
| Median event duration (s) | 0.01 | 0.01 | 0.01 | 0.01 | 0.03 | 0.03 | 0.02 | 0.02 | 0.01 | 0.01 | 0.01 | 0.01 |
| Standard deviation of event duration | 0.01 | 0.01 | 0.01 | 0.01 | 0.06 | 0.03 | 0.04 | 0.04 | 0.01 | 0.01 | 0.01 | 0.01 |
| Flood tide ($T_{bore}$ + 3600 s)[c] | | | | | | | | | | | | |
| Median event amplitude | 2.67 | 2.6 | 2.89 | 3 | 3.26 | 3.82 | 4.2 | 4.31 | 3.45 | 3.73 | 4.34 | 4.47 |
| Standard deviation of event amplitude | 2135.48 | 504.53 | 310.12 | 8647.76 | 507.38 | 3464.41 | 2153.2 | 1100.79 | 486.86 | 805.98 | 2309.77 | 1328.51 |
| Median event duration (s) | 0.03 | 0.03 | 0.03 | 0.03 | 0.02 | 0.01 | 0.01 | 0.01 | 0.01 | 0.01 | 0.01 | 0.01 |
| Standard deviation of event duration | 0.02 | 0.02 | 0.02 | 0.02 | 0.01 | 0.01 | 0.01 | 0.01 | 0.01 | 0.01 | 0.01 | 0.01 |

[a]Calculated based upon the first 10,000–60,000 events measured before the bore passage

[b]Calculated based upon the first 600 events after the rapid rise of the free-surface (approximately 20 s after bore passage)

[c]Calculated based upon the first 32,000 events at 3600 s after bore passage

**Table 4** Statistical properties of turbulent events during the late ebb tide flow, very early flood tide and flood tide phases on 29 August, 31 August and 27 October 2015 for the normal stress flux $v_x \times v_x$

| Date | 29/08/2015 | 31/08/2015 | 27/10/2015 |
|---|---|---|---|
| Total sampling duration (s) | 13,583 | 10,835 | 9861 |
| Initial water depth (m) | 1.685 | 1.12 | 1.24 |
| Froude number $Fr_1$ | 1.18 | 1.7 | 1.33 |
| Flux component | $v_x \times v_x$ | $v_x \times v_x$ | $v_x \times v_x$ |
| Total number of events | 286,598 | 245,703 | 258,167 |
| Initial flow conditions[a] | | | |
| Median event amplitude | 1.206 | 1.188 | 1.06 |
| Standard deviation of event amplitude | 1.372 | 1.257 | 1.01 |
| Median event duration (s) | 0.009 | 0.009 | 0.009 |
| Standard deviation of event duration | 0.005 | 0.005 | 0.008 |
| Very early flood tide ($T_{bore}$ + 20 s)[b] | | | |
| Median event amplitude | 1.011 | 1.073 | 0.965 |
| Standard deviation of event amplitude | 0.952 | 1.171 | 1.012 |
| Median event duration (s) | 0.008 | 0.015 | 0.008 |
| Standard deviation of event duration | 0.004 | 0.015 | 0.004 |
| Flood tide ($T_{bore}$ + 3600 s)[c] | | | |
| Median event amplitude | 0.907 | 0.914 | 0.885 |
| Standard deviation of event amplitude | 0.831 | 0.912 | 0.888 |
| Median event duration (s) | 0.015 | 0.009 | 0.008 |
| Standard deviation of event duration | 0.011 | 0.005 | 0.004 |

[a]Calculated based upon the first 40,000–60,000 events measured before the bore passage

[b]Calculated based upon the first 600 events after the rapid rise of the free-surface (approximately 20 s after bore passage)

[c]Calculated based upon the first 32,000 events at d after bore passage

## References


1. Bradshaw P (1971) An introduction to turbulence and its measurement. Pergamon Press, Oxford
2. Chanson H (2011) Tidal bores, aegir, eagre, mascaret, pororoca: theory and observations. World Scientific, Singapore. ISBN 9789814335416
3. Chanson H (2012) Momentum considerations in hydraulic jumps and bores. J Irrig Drain Eng ASCE 138(4):382–385. https://doi.org/10.1061/(ASCE)IR.1943-4774.0000409
4. Chanson H, Docherty NJ (2012) Turbulent velocity measurements in open channel bores. Eur J Mech B Fluids 32:52–58. https://doi.org/10.1016/j.euromechflu.2011.10.001
5. Chanson H, Reungoat D, Simon B, Lubin P (2011) High-frequency turbulence and suspended sediment concentration measurements in the Garonne River tidal bore. Estuar Coast Shelf Sci 95(2–3):298–306. https://doi.org/10.1016/j.ecss.2011.09.012
6. Faas RW (1995) Rheological constraints on fine sediment distribution and behavior: the Cornwallis Estuary, Novia Scotia. In: Proceedings of Canadian coastal conference, Dartmouth, pp 301–314
7. Fan D, Tu J, Shang S, Cai G (2014) Characteristics of tidal-bore deposits and facies associations in the Qiantang Estuary, China. Mar Geol 348:1–14. https://doi.org/10.1016/j.margeo.2013.11.012
8. Finnigan J (2000) Turbulence in plant canopies. Annu Rev Fluid Mech 32:519–571
9. Furgerot L, Mouaze D, Tessier B, Perez L, Haquin S, Weill P, Crave A (2016) Sediment transport induced by tidal bores. An estimation from suspended matter measurements in the Sée River (Mont-Saint-Michel Bay, northwestern France). C R Geosci 348:432–441
10. Goring DG, Nikora VI (2002) Despiking acoustic Doppler velocimeter data. J Hydraul Eng ASCE 128(1):117–126 **(Discussion: Vol. 129, No. 6, pp. 484-489)**

11. Greb SF, Archer AW (2007) Soft-sediment deformation produced by tides in a meizoseismic area, Turnagain Arm, Alaska. Geology 35(5):435–438
12. Johansson AV, Alfredsson PH (1982) On the structure of turbulent channel flow. J Fluid Mech 122:295–314
13. Kanani A, da Silva AMF (2015) Application of continuous wavelet transform to the study of large-scale coherent structures. Environ Fluid Mech 15:1293–1319. https://doi.org/10.1007/s10652-015-9428-x
14. Keevil CE, Chanson H, Reungoat D (2015) Fluid flow and sediment entrainment in the Garonne River bore and tidal bore collision. Earth Surf Process Landf 40(12):1574–1586. https://doi.org/10.1002/esp.3735
15. Kline SJ, Reynolds WC, Schraub FA, Runstaller PW (1967) The structure of turbulent boundary layers. J Fluid Mech 30(4):741–773
16. Koch C, Chanson H (2009) Turbulence measurements in positive surges and bores. J Hydraul Res IAHR 47(1):29–40. https://doi.org/10.3826/jhr.2009.2954
17. Lohrmann A, Cabrera R, Kraus NC (1994) Acoustic-doppler velocimeter (ADV) for laboratory use. In: Pugh CA (ed) Proceedings of the conference fundamentals and advancements in hydraulic measurements and experimentation. ASCE, Buffalo, pp 351–365
18. Lozano-Durab A, Flores O, Jimenez J (2012) The three-dimensional structure of momentum transfer in turbulent channels. J Fluid Mech 694:100–130. https://doi.org/10.1017/jfm.2011.524
19. Nakagawa H, Nezu I (1981) Structure of space–time correlations of bursting phenomena in an open-channel flow. J Fluid Mech 104:1–43
20. Narasimha R, Kumar SR, Prabhu A, Kailas SV (2007) Turbulent flux events in a nearly neutral atmospheric boundary layer. Philos Trans R Soc Ser A 365:841–858
21. Nezu I (2005) Open-channel flow turbulence and its research prospect in the 21st century. J Hydraul Eng ASCE 131(4):229–246
22. Nezu I, Nakagawa H (1993) Turbulence in open-channel flows. IAHR Monograph, IAHR Fluid Mechanics Section, Balkema Publ., Rotterdam
23. Nikora VI (1999) Origin of the " − 1" spectral law in wall-bounded turbulence. Phys Rev Lett 83(4):734–736
24. Nortek AS (2009) Vectrino velocimeter user guide. Nortek AS, Vangkroken
25. Osterlund JM, Lindgren B, Johansson AV (2003) Flow structures in zero pressure-gradient turbulent boundary layers at high Reynolds numbers. Eur J Mech B Fluids 22:379–390. https://doi.org/10.1016/S0997-7546(03)00034-7
26. Perry AE, Lim KL, Henbest SM (1987) An experimental study of the turbulence structure in smooth- and rough-wall boundary layers. J Fluid Mech 177:437–466
27. Piquet J (1999) Turbulent flows. Models and physics. Springer, Berlin
28. Rahman S (2002) Effect of bed roughness on scalar mixing in turbulent boundary layer, Ph.D. Thesis. Georgia Inst. of Tech
29. Rao KN, Narasimha R, Narayanan AAB (1971) The "bursting" phenomena in a turbulent boundary layer. J Fluid Mech 48(Part 2):339–352
30. Reungoat D, Chanson H, Caplain B (2014) Sediment processes and flow reversal in the undular tidal bore of the Garonne River (France). Environ Fluid Mech 14(3):591–616. https://doi.org/10.1007/s10652-013-9319-y
31. Reungoat D, Chanson H, Keevil CE (2015) Field measurements of unsteady turbulence in a tidal bore: the Garonne River in October 2013. J Hydraul Res IAHR 53(3):291–301. https://doi.org/10.1080/00221686.2015.1021717
32. Reungoat D, Leng X, Chanson H (2016) Hydrodynamic and sedimentary processes of tidal bores: Arcins channel, Garonne River in August–September–October 2015, Hydraulic Model Report No. CH102/16. School of Civil Engineering, The University of Queensland, Brisbane
33. Schlichting H (1979) Boundary layer theory, 7th edn. McGraw-Hill, New York
34. Simpson JH, Fisher NR, Wiles P (2004) Reynolds stress and TKE production in an estuary with a tidal bore. Estuar Coast Shelf Sci 60(4):619–627
35. Trevethan M, Chanson H (2010) Turbulence and turbulent flux events in a small estuary. Environ Fluid Mech 10(3):345–368. https://doi.org/10.1007/s10652-009-9134-7
36. Tricker RAR (1965) Bores, breakers, waves and wakes. American Elsevier Publ. Co., New York
37. Wahl TL (2003) Despiking acoustic Doppler velocimeter data. Discussion. J Hydraul Eng ASCE 129(6):484–487
38. Wallace JM (2013) Highlights from 50 years of turbulent boundary layer research. J Turbul 13(53):1–70
39. Wolanski E, Williams D, Spagnol S, Chanson H (2004) Undular tidal bore dynamics in the Daly Estuary, Northern Australia. Estuar Coast Shelf Sci 60(4):629–636